Parametric Amplification of a Superconducting Plasma Wave

S. Rajasekaran[1,2], E. Casandruc[1,2], Y. Laplace[1,2], D. Nicoletti[1,2], G. D. Gu[3], S. R. Clark[4,5,1], D. Jaksch[5,6], A. Cavalleri[1,2,5,*]

[1]*Max Planck Institute for the Structure and Dynamics of Matter, Luruper Chaussee 149, 22761 Hamburg, Germany*
[2]*Center for Free-Electron Laser Science, Luruper Chaussee 149, 22761 Hamburg, Germany*
[3]*Condensed Matter Physics and Materials Science Department, Brookhaven National Laboratory, Upton, New York 11973-5000, USA*
[4]*Department of Physics, University of Bath, Claverton Down, BA2 7AY, Bath United Kingdom*
[5]*Department of Physics, Oxford University, Clarendon Laboratory, Parks Road, OX1 3PU Oxford, United Kingdom*
[6]*Centre for Quantum Technologies, National University of Singapore, 3 Science Drive 2, Singapore 117543, Singapore*
**e-mail: andrea.cavalleri@mpsd.mpg.de*

Supplementary Information

S1: Scheme of the experimental geometry

A schematic representation of the experimental geometry is shown in Fig. S1. The *ac*-cut surface of a LBCO (x=9.5%) sample was illuminated with pump and probe THz pulses, both polarized along the *c* direction (*i.e.*, perpendicular to the Cu-O layers). The probe beam had an incidence angle of 45°, while the pump hit the sample at normal incidence.

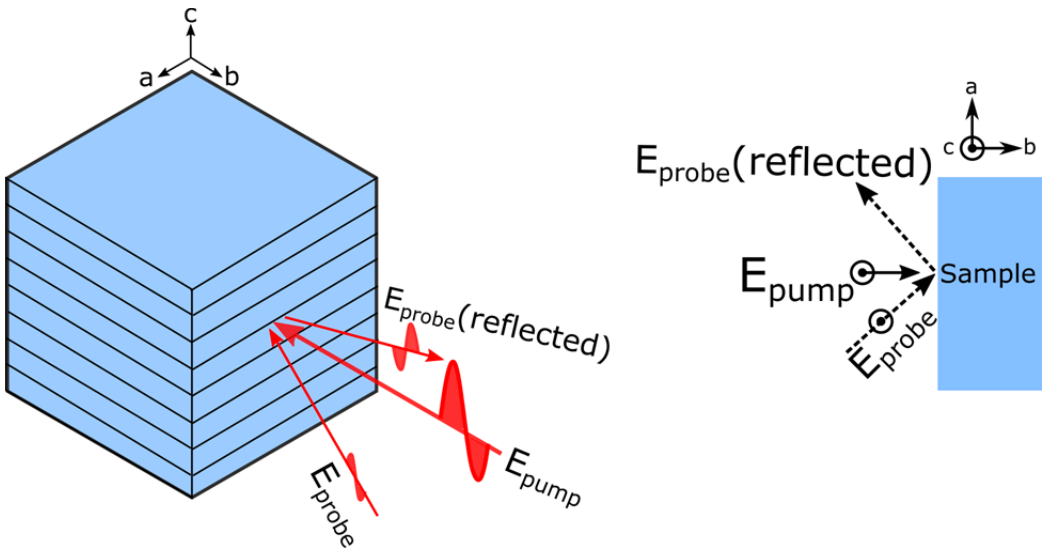

Figure S1. Schematic representation of the measurement geometry. The Cu-O planes are indicated along with propagation vector and polarization of the light fields. A top view is shown on the right.

S2. Josephson equation as Mathieu equation

A Josephson junction can be approximated with an LC circuit equivalent. By equating the capacitive current $\left(I_c = C\frac{\partial V}{\partial t} \right)$ to the inductive tunneling current $\left(-I_L = -I_0 \sin\theta_{i,i+1}(t) \right)$ and using then the second Josephson equation $\left(\frac{\partial[\theta_{i,i+1}(t)]}{\partial t} = \frac{2eV}{\hbar} \right)$ we obtain the temporal dependence of the Josephson phase $(\theta_{i,i+1}(t))$ as

$$-\frac{\varepsilon_r}{c^2}\frac{\partial^2\theta_{i,i+1}(x,t)}{\partial t^2}=\frac{\omega_p^2\varepsilon_r}{c^2}\sin\theta_{i,i+1}(x,t) \quad (1)$$

where ε_r is the dielectric permittivity of the Josephson junction, c the speed of light, e the electronic charge, I_0 the critical current, C the capacitance of the junction, and

$$\omega_p^2=\omega_0^2=\frac{2I_0e}{\hbar C}.$$

The equation of motion of the Josephson phase with damping (γ) therefore reads

$$-\frac{1}{\gamma}\frac{\partial\theta_{i,i+1}(x,t)}{\partial t}-\frac{\varepsilon_r}{c^2}\frac{\partial^2\theta_{i,i+1}(x,t)}{\partial t^2}=\frac{\omega_p^2\varepsilon_r}{c^2}\sin\theta_{i,i+1}(x,t) \quad (2)$$

In a perturbed state in which the oscillator strength is modified as

$$f(t)\sim\omega_p^2(t)\approx\omega_0{}^2\left(1-\frac{\theta_0^2+\theta_0^2\cos(2\omega_0t)}{4}\right) \quad (3)$$

the time dependence of the Josephson phase is described by

$$\frac{\varepsilon_r}{c^2}\frac{\partial^2\theta_{probe}(x,t)}{\partial t^2}+\frac{1}{\gamma}\frac{\partial\theta_{probe}(x,t)}{\partial t}+\frac{\omega_0^2\varepsilon_r}{c^2}\left(1-\frac{\theta_0^2+\theta_0^2\cos(2\omega_0t)}{4}\right)\theta_{probe}(x,t)=0 \quad (4)$$

We note that Eq. (4) is a damped Mathieu equation of the form

$$\frac{\partial^2\theta_{probe}(x,t)}{\partial t^2}+\beta\frac{\partial\theta_{probe}(x,t)}{\partial t}+\left(a-\alpha\cos(2\omega_0(t)\right)\theta_{probe}(x,t)=0 \quad (5)$$

where $a=\left(1-\frac{\theta_0^2}{4}\right)\omega_0^2$, $\alpha=\frac{\theta_0^2\cos(2\omega_0t)}{4}\omega_0^2$ and $\beta=\frac{c^2}{\varepsilon_r\gamma}$.

S3. Simulation of the nonlinear optical properties from the sine-Gordon equation

A Josephson junction with semi-infinite layers stacked along the *z* direction (with translational invariance along the *y* direction) can be modeled with the one-

dimensional sine-Gordon equation[1,2]. Being x the propagation direction, the Josephson phase evolution is described by:

$$\frac{\partial^2\theta_{i,i+1}(x,t)}{\partial x^2}-\frac{1}{\gamma}\frac{\partial\theta_{i,i+1}(x,t)}{\partial t}-\frac{\varepsilon_r}{c^2}\frac{\partial^2\theta_{i,i+1}(x,t)}{\partial t^2}=\frac{\omega_p^2\varepsilon_r}{c^2}\sin\theta_{i,i+1}(x,t) \quad (6)$$

The damping factor γ is a fitting parameter used to reproduce the optical properties observed experimentally. In this section, we drop the subscripts for simplicity, *i.e.* we redefine $\theta_{i,i+1}(x,t)=\theta(x,t)$. The pump and probe THz fields impinge on the superconductor at the boundary $x=0$. The Josephson phase evolution is therefore affected by the following boundary conditions at the vacuum-sample interface[3].

$$[\mathrm{E_i(t)}+\mathrm{E_r(t)}]_{\mathrm{x=-0}}=\mathrm{E_c(x,t)}|_{\mathrm{x=+0}}=\mathrm{H_0}\frac{1}{\omega_{\mathrm{JPR}}\sqrt{\varepsilon}}\frac{\partial\theta(\mathrm{x,t})}{\partial\mathrm{t}}|_{\mathrm{x=+0}}, \quad (7)$$

$$[\mathrm{H_i(t)}+\mathrm{H_r(t)}]_{\mathrm{x=-0}}=\mathrm{H_c(x,t)}|_{\mathrm{x=+0}}=-\mathrm{H_0}\lambda_{\mathrm{J}}\frac{\partial\theta(\mathrm{x,t})}{\partial\mathrm{x}}|_{\mathrm{x=+0}}. \quad (8)$$

The subscripts *i*, *r*, and *c* denote the fields incident, reflected and propagating inside the cuprate, respectively. Here $\mathrm{H_0}=\Phi_0/2\pi\mathrm{D}\lambda_{\mathrm{J}}$, where Φ_0 is the flux quantum $\left(\Phi_0=\frac{hc}{2e}\right)$ and D is the distance between adjacent superconducting layers. The equilibrium Josephson Plasma Resonance (JPR) is an input parameter in the simulations, which is chosen to be that of $La_{1.905}Ba_{0.095}CuO_4$, *i.e.* $\omega_{\mathrm{JPR}}=0.5$ THz.

For fields in vacuum ($x<0$), the Maxwell's equations imply

$$\mathrm{E_i}-\mathrm{E_r}=\frac{\omega\mu}{\mathrm{ck}}(\mathrm{H_i}+\mathrm{H_r})=\mathrm{H_i}+\mathrm{H_r}\,. \quad (9)$$

By combining Eq. (9) with Eq. (7) and (8) we obtain the boundary condition

$$\frac{2\sqrt{\varepsilon}}{\mathrm{H_0}}\mathrm{E_i(t)}|_{\mathrm{x=-0}}=\frac{\partial\theta(\mathrm{x,t})}{\omega_{\mathrm{JPR}}\,\partial\mathrm{t}}|_{\mathrm{x=+0}}-\sqrt{\varepsilon}\frac{\partial\theta(\mathrm{x,t})}{\partial\mathrm{x}/\lambda_{\mathrm{J}}}|_{\mathrm{x=+0}}. \quad (10)$$

After solving the Josephson phase through Eq. (6) and Eq. (10), the reflected field is calculated from Eq. (7). The equilibrium reflectivity of the cuprate is obtained by computing the ratio between the Fourier transforms of the reflected field and a weak input field

$$\mathrm{r}^{\mathrm{equilibrium}}(\omega) = \mathrm{E}_{\mathrm{r}}^{\mathrm{equilibrium}}(\omega)/\mathrm{E}_{\mathrm{i}}(\omega)\,. \tag{11}$$

The complex optical properties are then calculated from $\mathrm{r}^{\mathrm{equilibrium}}(\omega)$. In particular, the equilibrium dielectric permittivity and loss function are computed as:

$$\varepsilon(\omega) = \left(\left(\frac{1-\mathrm{r}^{\mathrm{equilibrium}}(\omega)}{1+\mathrm{r}^{\mathrm{equilibrium}}(\omega)}\right)^2\right)$$

$$\mathrm{L}(\omega) = -\mathrm{Imag}\left(\left(\frac{\mathrm{r}^{\mathrm{equilibrium}}(\omega)+1}{\mathrm{r}^{\mathrm{equilibrium}}(\omega)-1}\right)^2\right)$$

For the pump-probe configuration, the input field is the sum of the pump and probe fields (with a defined delay between them):

$$\mathrm{E}_{\mathrm{i}}(\mathrm{t}) = \mathrm{E}_{\mathrm{pump}}(\mathrm{t}) + \mathrm{E}_{\mathrm{probe}}(\mathrm{t}). \tag{12}$$

Correspondingly, the Josephson phase can be written as

$$\theta = \theta_{\mathrm{pump}} + \theta_{\mathrm{probe}}. \tag{13}$$

And the sine-Gordon equation (6) decomposes into two coupled equations

$$\frac{\partial^2\theta_{pump}(x,t)}{\partial x^2} - \frac{1}{\gamma}\frac{\partial\theta_{pump}(x,t)}{\partial t} - \frac{\varepsilon_r}{c^2}\frac{\partial^2\theta_{pump}(x,t)}{\partial t^2} = \frac{\omega_p^2\varepsilon_r^2}{c^2}\sin\theta_{pump}(x,t)\cos\theta_{probe}(x,t) \tag{14}$$

$$\frac{\partial^2\theta_{probe}(x,t)}{\partial x^2} - \frac{1}{\gamma}\frac{\partial\theta_{probe}(x,t)}{\partial t} - \frac{\varepsilon_r}{c^2}\frac{\partial^2\theta_{probe}(x,t)}{\partial t^2} = \frac{\omega_p^2\varepsilon_r^2}{c^2}\sin\theta_{probe}(x,t)\cos\theta_{pump}(x,t) \tag{15}$$

For a weak probe ($\theta \ll 1$), $\cos\theta_{probe} \approx 1$ and the effect of θ_{probe} on θ_{pump} can be neglected in Eq. (14). The phases θ_{pump} and θ_{probe} are calculated in two steps: (i) Eqs. (14) and (10) are solved with the driving field $E_i = E_{pump}$ to get $\theta_{pump}(x,t)$ and then (ii) Eq. (15) and (10) are solved by substituting $\theta_{pump}(x,t)$ with the input field $E_i = E_{probe}$, to obtain $\theta_{probe}(x,t)$ and the reflected probe field $E_r^{perturb}$. The perturbed reflectivity is given by

$$r^{perturb}(\omega,t) = E_r^{perturb}(\omega,t)/E_i(\omega). \quad (16)$$

The optical response functions of the perturbed material are extracted from the complex optical reflectivity $r^{perturb}$. For instance, the dielectric permittivity and loss function are calculated as:

$$\varepsilon(\omega) = \left(\left(\frac{1-r^{perturb}(\omega)}{1+r^{perturb}(\omega)}\right)^2\right)$$

$$L(\omega,t) = -\mathrm{Imag}\left(\left(\frac{r^{perturb}(\omega,t)+1}{r^{perturb}(\omega,t)-1}\right)^2\right).$$

S4. Pump spectrum

The electric field profile of the THz pump pulse measured at the sample position is displayed in Fig. S2A along with the corresponding frequency spectrum (Fig. S2B). This is peaked at ~0.5 THz, being therefore resonant with the JPR of $LBCO_{9.5}$ (see reflectivity edge in the blue curve of Fig. S2B). The input pump field used in the simulations is also displayed (dashed), both in time (Fig. S2A) and frequency domain (Fig. S2B).

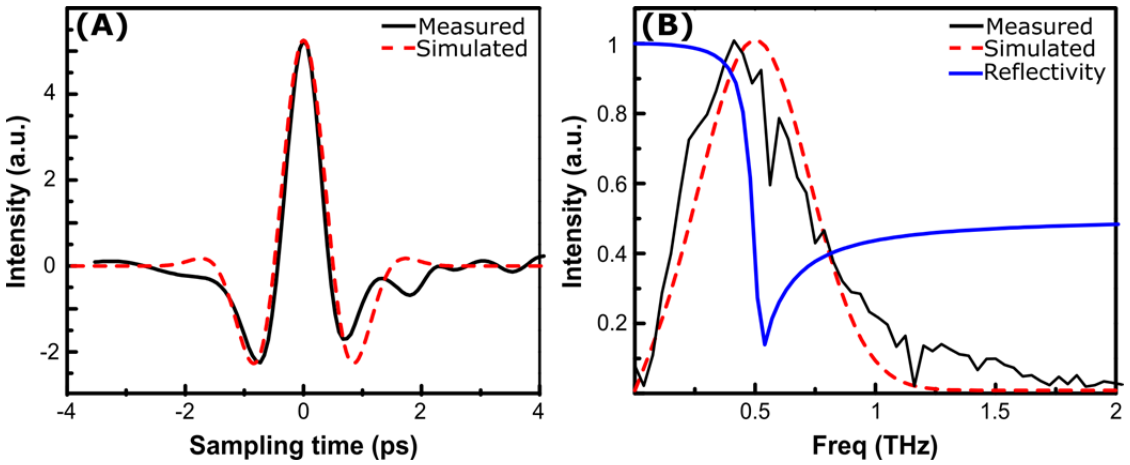

Figure S2. (**A**) Electro-optic sampling trace of the THz pump pulse measured at the sample position and (**B**) corresponding frequency spectrum. The *c*-axis equilibrium reflectivity of $LBCO_{9.5}$ at T = 5 K is also displayed. Dashed lines in both panels refer to the input pump field used in simulations. The ringing observed on the trailing edge of the pulse (black line in **A**) is due to narrow water absorption lines at ~0.5 THz and ~1.2 THz (see also corresponding spectrum in **B**). These can be ignored because all measurements but that reported in this figure have been performed under high vacuum condition ($P = 10^{-6}$ mbar).

S5. Pump field dependence

The spectrally integrated pump-probe response is displayed in Fig. S3 for different pump field strengths. A minimum field of ~30 kV/cm was required to induce a response of sufficient amplitude to be detected in our experiment.

The oscillatory behavior at twice the equilibrium JPR frequency was found to be only weakly dependent on the pump field strength. Note that pump-field-independent $2\omega_{JP0}$ oscillations are only observed at $t \gtrsim 0$ ps, *i.e.* after the early-time dynamics ($t \lesssim 0$ ps) dominated by perturbed free induction decay[4,5,6] (shaded region in Fig. S3).

The time-delay and frequency dependent loss function measured with a pump field of 40 kV/cm is displayed in Fig. S4, along with the corresponding theoretical calculations. These can be compared with the data of Fig. 5 in the main text, which were taken with a higher pump field (~80 kV/cm). Remarkably, while the $2\omega_{JP0}$ oscillatory behavior is observed in both data sets, periodic amplification is only present with stronger pump field (consistently in both experiment and calculations).

This indicates that phase-sensitive amplification of Josephson Plasma Wave can be achieved only for THz pump field amplitudes above a threshold of ~70 kV/cm.

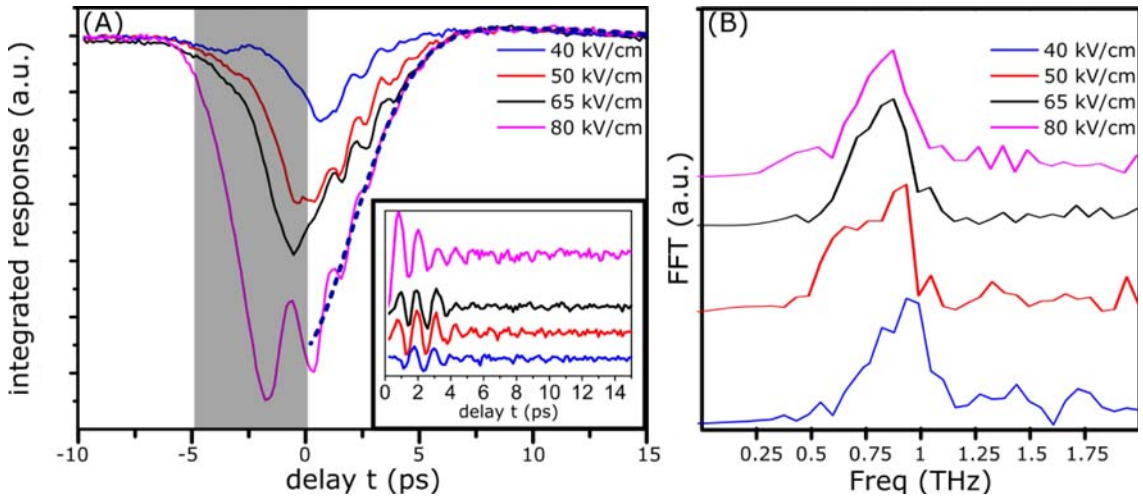

Figure S3. (**A**) Spectrally-integrated pump-probe response measured for different pump field strengths at a sample temperature T = 5 K. The dashed line is an example of background which was subtracted to extract the oscillatory components shown in the inset. The negative time delay region, interested by perturbed free induction decay, is shaded in grey. (**B**) Normalized Fourier transforms of the oscillatory signals.

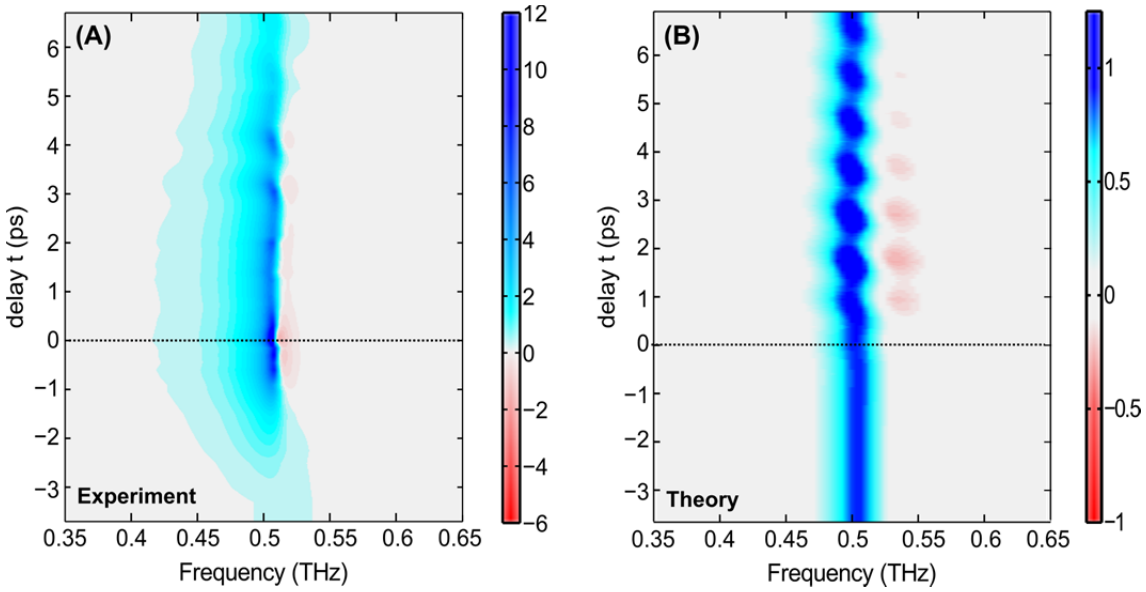

Figure S4. Time-delay and frequency dependent loss function determined (**A**) experimentally and (**B**) by numerically solving the sine-Gordon equation in nonlinear regime. The applied THz pump field is 40 kV/cm.

S6. Temperature dependence

In Fig. S5 we show the measured equilibrium reflectivity of $LBCO_{9.5}$ at two different temperatures. The JPR exhibits a red shift from ~0.5 THz to ~0.35 THz upon increasing the sample temperature from 5 K to 30 K.

The temperature dependence of the spectrally integrated pump-probe response has also been determined experimentally (only the oscillatory component of this response is shown in Fig. S5B). As expected, the measured oscillations slow down with increasing *T*. Indeed their frequency reduces from ~ 1 THz at 5 K to ~0.75 THz at 30 K, scaling as $2\omega_{JP0}$.

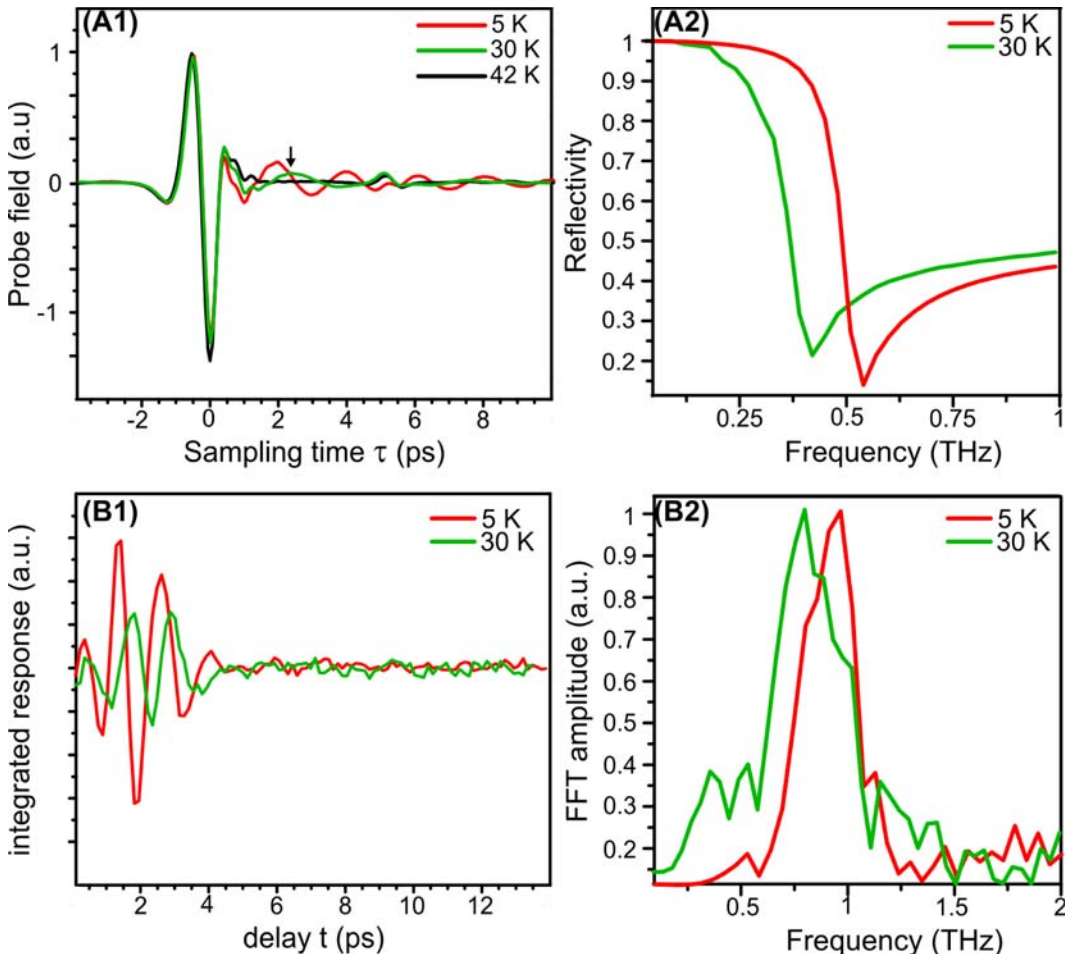

Figure S5. (**A1**) $E_{probe}(\tau)$ measured in absence of pump field at different temperatures above and below T_c. (**A2**) Frequency-dependent reflectivity at T = 5 K and T = 30 K, extracted from the $E_{probe}(\tau)$ trace of panel (**A1**). (**B1**) Oscillatory component of the spectrally-integrated pump-probe response, measured at T = 5 K and T = 30 K at the same τ (arrow in (**A1**)). (**B2**) Corresponding Fourier transforms of the oscillatory integrated response.

S7. Parametric Amplification

An increase of the signal amplitude along the sampling time axis τ, which is in fact the Fourier transform of the spectrum, is shown in Fig. 4 of the main text. Amplification is demonstrated even more directly in Fig. 5, where we show the energy loss function. As discussed in the text, this function is proportional to $\varepsilon_2(\omega)$, and it is shown to become negative at selected time delays.

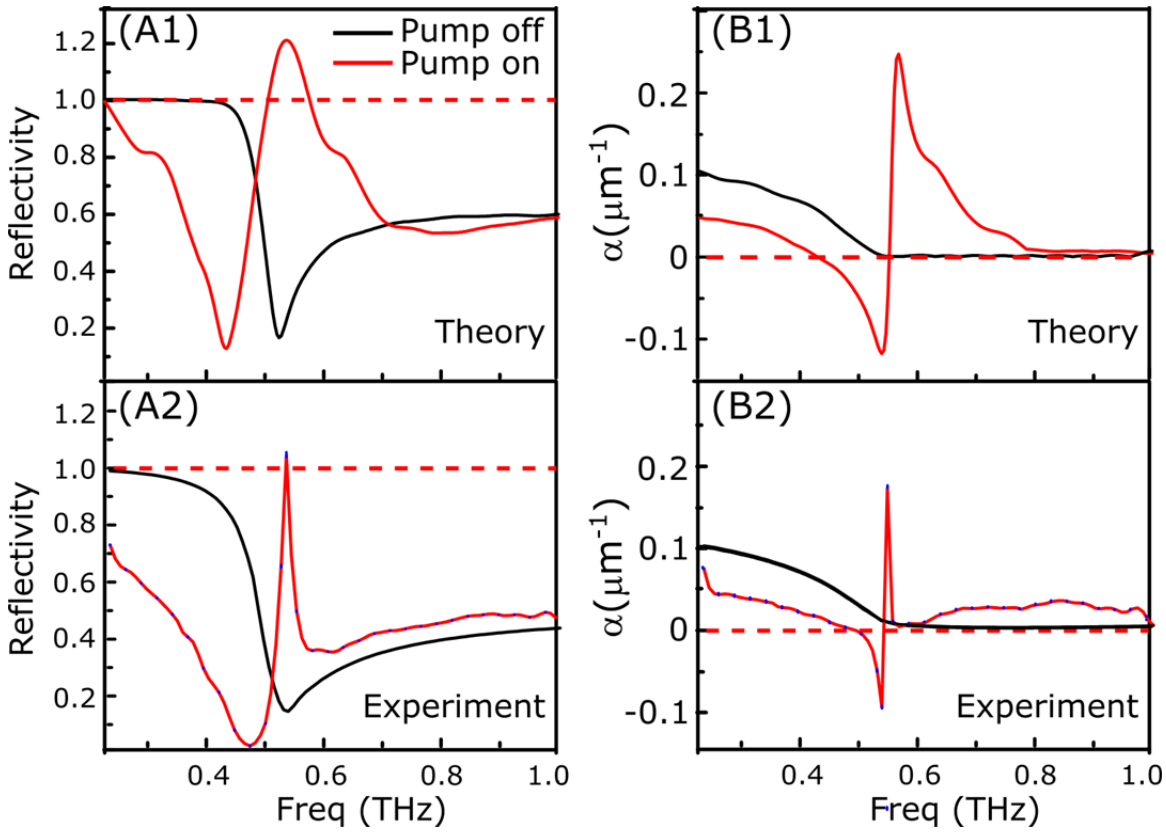

Figure S6. (**A**) Frequency-dependent reflectivity and (**B**) corresponding absorption coefficient, determined before and after excitation (at a selected pump-probe delay *t*). Experimental data (**A2**, **B2**) are displayed along with simulations (**A1**, **B1**), consistently showing amplification at $\omega \sim \omega_{JP0}$. Dashed lines at R = 1 and α = 0 are visualized to emphasize the amplification. Error bars (blue ticks in **A2**, **B2**) are propagated from the standard deviation in the measured $\Delta E_R/E_R$ signal (estimated from different scans).

In order to quantify the level of amplification, we use the absorption coefficient α, as in Ref. 7. The lowest value determined at ω_{JP0} is $\alpha = \frac{2\omega}{c}\mathrm{Im}(\tilde{n}) \simeq (-0.090 \pm 0.003)\mu\mathrm{m}^{-1}$

(here $\tilde{n}$ is the complex refractive index), as shown in the Fig. S6B for both experiment and simulations.

For clarity, we also include the reflectivity in Fig. S6A, which for a specific frequency becomes larger than 1 ($R = 1.042 \pm 0.008$), providing a further demonstration of amplification.

References

1. Hu, X. & Lin, S.-Z. Phase dynamics in a stack of inductively coupled intrinsic Josephson junctions and terahertz electromagnetic radiation. *Supercond. Sci. Technol.* **23,** 053001 (2010).
2. Dienst, A. *et al.* Optical excitation of Josephson plasma solitons in a cuprate superconductor. *Nat. Mater.* **12,** 535–541 (2013).
3. Savel'ev, S., Yampol'skii, V. A., Rakhmanov, A. L. & Nori, F. Terahertz Josephson plasma waves in layered superconductors: spectrum, generation, nonlinear and quantum phenomena. *Rep. Prog. Phys.* **73,** 026501 (2010).
4. Kindt, J. T. & Schmuttenmaer, C. A. Theory for determination of the low-frequency time-dependent response function in liquids using time-resolved terahertz pulse spectroscopy. *J. Chem. Phys.* **110,** 8589–8596 (1999).
5. Beard, M. C., Turner, G. M. & Schmuttenmaer, C. A. Transient photoconductivity in GaAs as measured by time-resolved terahertz spectroscopy. *Phys. Rev. B* **62,** 15764–15777 (2000).
6. Hamm, P. Coherent effects in femtosecond infrared spectroscopy. *Chem. Phys.* **200,** 415–429 (1995).
7. Huber R. *et al.,* Stimulated Terahertz Emission from Intraexcitonic Transitions in Cu_2O. *Phys. Rev. Lett.* **96**, 017402 (2006).